Ultrafast Protein Dynamics of Bacteriorhodopsin Probed by Photon Echo and Transient Absorption Spectroscopy

ARTICLE *in* THE JOURNAL OF PHYSICAL CHEMISTRY B · JUNE 2002

Impact Factor: 3.3 · DOI: 10.1021/jp014681b

6 AUTHORS, INCLUDING:

Delmar S Larsen
University of California, Davis
86 PUBLICATIONS **2,706** CITATIONS

SEE PROFILE

Marc Tancredi Facciotti
University of California, Davis
53 PUBLICATIONS **1,812** CITATIONS

SEE PROFILE

Ultrafast Protein Dynamics of Bacteriorhodopsin Probed by Photon Echo and Transient Absorption Spectroscopy

John T. M. Kennis,*,†,# Delmar S. Larsen,†,# Kaoru Ohta,†,†† Marc T. Facciotti,§ Robert M. Glaeser,‡,∥,⊥ and Graham R. Fleming*,†,∥

Department of Chemistry, Department of Molecular and Cell Biology, Graduate Group in Biophysics, University of California, Physical Biosciences Division, Life Sciences Division, Lawrence Berkeley National Laboratory, Berkeley, California 94720

Received: December 31, 2001; In Final Form: April 5, 2002

Bacteriorhodopsin (bR) is an efficient light-driven proton pump which shows a trans-cis isomerization reaction of its retinal chromophore after light absorption. BR exhibits a large reorganization energy λ of 2520 cm^{-1} on optical excitation. In this paper, we have studied the nature, origin, and dynamical aspects of this extensive reorganization. We report the results of a femtosecond three-pulse echo peak shift (3PEPS), transient grating (TG) and transient absorption (TA) study, complemented with those of steady-state absorption and fluorescence spectroscopy in wild-type bR and the D85S mutant in its blue and purple, halide-pumping forms. We have simulated the results in the context of the multimode Brownian oscillator (MBO) formalism. A simple model that incorporates retinal's known intramolecular vibrations, which represent 1094 cm^{-1} or reorganization energy, and a single Gaussian protein relaxation with a decay of 50 fs representing 1430 cm^{-1} of reorganization energy, yielded satisfactory results for all linear and nonlinear experimental results on wild-type bR. For the D85S mutant in its blue form, the same model could be applied with a Gaussian relaxation of 1050 cm^{-1} amplitude. It is concluded that the protein environment of the retinal chromophore only exhibits an inertial response, and does not show any diffusive-type motions on a sub-ps to ps time scale, which is probably a consequence of the covalently constrained, polymeric nature of the protein. Our results are in close agreement with earlier molecular dynamics simulations on bR (Xu, D.; Martin, C. H.; Schulten, K. *Biophys. J.* **1996**, *70*, 453−460), which indicated that after retinal excitation, which is accompanied by a significant charge relocation along the polyene backbone, the protein exhibits an extensive dielectric relaxation on a 100 fs time scale representing an energy change of ∼1700 cm^{-1}. We conclude that on the sub-ps to ps timescale, the protein's major influence is electrostatic via a large number of small-amplitude motions of charges and dipoles. Major structural rearrangements of the protein do not occur on the timescale of isomerization. Polarized transient absorption measurements on bR and the D85S mutant indicated a time-independent anisotropy of the stimulated emission of 0.35, indicating that in the excited state, no change of the direction of the transition dipole moment of retinal takes place during the excited-state lifetime.

1. Introduction

The light-induced reactions in biological photoreceptors can take place at remarkable rates and efficiencies. A well-known example of such a photoreceptor is bacteriorhodopsin (bR), a photosynthetic protein found in the purple membrane of the Archaeon *Halobacterium salinarum*. Upon illumination, bR translocates protons toward the endoplasm of the cell (for recent reviews, see refs 1,2). It binds retinal as a chromophore, which assumes an all-trans geometry in the ground state, and exhibits a trans-cis isomerization upon optical excitation. This event triggers a series of intraprotein proton transfers, accompanied by distinct and discrete structural changes in the protein, and ultimately a proton is pumped across the membrane. The resulting transmembrane proton gradient in turn drives ATP synthesis through the action of ATP synthase.

The outcome of a photochemical reaction in the condensed phase depends on the nature of the reacting chromophore and its environment, which may for instance be a liquid, glass or a protein. In the recent past, there has been an extensive effort to characterize and understand solvation dynamics, i.e., the response of liquid solvents to the creation of an excited state on a chromophore.[3,4] The advent of sub-100 fs, stable laser systems enabled the development of spectroscopic techniques such as fluorescence upconversion and photon echo spectroscopy. In combination with detailed modeling including molecular dynamics simulations[4] and nonlinear spectroscopic approaches,[5−8] the application of these techniques has led to a large progress in properly characterizing and understanding the time scales and nature of the different solvation components in the liquid phase. Two components in solvation in liquids could be distinguished: a fast inertial response, occurring on a time scale less than 100 fs, followed by a slower, diffusive component on a picosecond time scale. The inertial response often accounts

* To whom correspondence should be addressed. E-mail: john@nat.vu.nl. Fax: +31204447999, or E-mail: GRFleming@lbl.gov. Fax: (510)642-6340.

† Department of Chemistry, University of California.

‡ Department of Molecular and Cell Biology, University of California.

§ Graduate Group in Biophysics, University of California.

∥ Physical Biosciences Division, Lawrence Berkeley National Laboratory.

⊥ Life Sciences Division, Lawrence Berkeley National Laboratory.

Present address: Department of Biophysics and Physics of Complex Systems, Faculty of Sciences, Vrije Universiteit, Amsterdam, The Netherlands.

†† Present address: Department of Chemistry, Kobe University, Japan.

10.1021/jp014681b CCC: $22.00
Published on Web 05/09/2002

for half the total reorganization energy or more, and entails independent, underdamped motion of the solvent molecules in their native potential wells. The diffusive component represents the reorientation of the solvent molecules into a new equilibrium, whereby the nuclei may hop between different potential wells. It involves collective motions of the solvent molecules, like librations and large rotations. It is thought that the diffusive solvent rearrangement plays an important role in chemical reactivity, as it may reduce reaction barriers and stabilize reaction intermediates.[9]

BR undergoes a light-induced photocycle involving discrete reaction intermediates referred to as K, L, etc. through O, after which the protein returns to its all-trans retinal ground state. The K intermediate corresponds to the 13-cis isomerized form of retinal.[12,14] An early photocycle intermediate preceding the 13-cis isomer K has been identified, J, which is formed in ~500 fs and has a lifetime of 3 ps; Conflicting views exist on the nature of J, i.e., whether it corresponds to the all-trans[14] or isomerized conformation of retinal.[10−13] Despite these controversies, it is firmly established that the trans-to-cis isomerization of retinal in bR is an ultrafast process which occurs with a 65% quantum efficiency and takes place exclusively about the C_{13}=C_{14} double bond.[15,16,17] The situation in bR contrasts starkly with retinal in solution where the light-induced isomerization reaction is only ~15% efficient and may occur about any of the double bonds near the Schiff base terminus.[18] The protein environment of the retinal chromophore thus plays an important role in achieving high selectivity and efficiency in bR, and it has been shown that site-directed mutants of bR with altered residues near the retinal chromophore exhibit a decreased isomerization reaction rate.[19]

BR's photochemistry has been studied extensively with a variety of techniques, and the isomerization reaction has primarily been described in terms of retinal's intramolecular reaction coordinates, especially the torsion and stretching of the C_{13}=C_{14} bond.[11,20−25] Despite the protein's obvious defining role on bR's photochemistry, the protein dynamics upon excitation of retinal have largely remained *terra incognita*. Does the protein dynamics exhibit "inertial" and "diffusive" components, like liquids? (Throughout the paper, we will refer to these protein dynamics as "protein solvation", in analogy to the situation in liquids) If so, on what time scales do these processes take place? How much energy flows into protein solvation modes? Can such a protein solvation process possibly be correlated with a stabilization of a transition state on bR's efficient reaction pathway? To address these questions, we have performed a broad study encompassing three-pulse echo peak shift (3PEPS), transient grating (TG), transient absorption (TA), steady-state absorption and fluorescence spectroscopy on bR. Moreover, we present results on the blue D85S mutant, which exhibits dramatically altered excited state properties similar to those of acid blue or deionized wild type bR. We analyze the linear and nonlinear data within the framework of the Multimode Brownian Oscillator (MBO) model, explicitly taking into account the intramolecular modes of retinal in bR. This holistic approach allows for a definite assignment of contributions by retinal's intramolecular modes, protein solvation components and excited-state lifetimes in the signals, thus giving a complete picture of all dynamic aspects that are interrogated with the utilized spectroscopies.

2. Experimental Section

The bR used for the fluorescence and TA measurements was prepared as described previously,[26] and the bR samples used for the 3PEPS and TG experiments were purchased from Sigma-Aldrich Chemicals. The purple membranes were suspended in a 100 mM HEPES buffer at pH 8.0. All bR samples were light-adapted by illumination on top of an overhead projector for 30 min prior to the measurements, and kept in that state by continuous illumination during the measurements. The site-directed mutagenesis technique used to construct the D85S mutant is described elsewhere.[27] For the D85S mutant in its blue form, the membranes were suspended in a 20 mM potassium phosphate buffer at pH 8.3. For the D85S mutant in its purple, halide-pumping form, the membranes were suspended in a 20 mM potassium phosphate buffer at pH 5.0, and a 3 M KCl solution was added to a final concentration of 1 M for the fluorescence and absorption measurements, or 300 mM for the TA measurements.

For the time-resolved measurements, the samples were loaded into a flow system with a 1 mm path length (TA measurements) or a 0.2 mm path length (3PEPS and TG measurements) flow cuvette, cooled to 10 °C and flowed at a rate of 0.5 to 1 m/s. The absorbance was about 0.3 per mm at the excitation wavelength for the TA measurements, and 0.15 per 0.2 mm for the 3PEPS and TG experiments.

Absorption spectra were recorded on a commercial spectrophotometer (Shimadzu). Steady-state fluorescence was measured on a commercial fluorimeter equipped with a double monochromator (SPEX Fluorolog 3, Jobin-Yvon) in a front-face detection geometry. The low fluorescence quantum yield (10^{-5}−10^{-4}) of bR[28,29] required special precautions to minimize or eliminate unwanted background signals. To minimize Raman scattering from the aqueous buffer, the samples were concentrated and contained in a thin cuvette of 0.2 mm path length with a maximum absorbance of 0.3. A 200 μW beam with an area of 0.5 cm^2 was used for excitation, and a long-pass filter with a cutoff wavelength at 620 nm was put in front of the detector to eliminate scattered pump light. To prevent the buildup of photocycle intermediates, the sample cuvette was mounted on a stage, which was continuously translated in a linear motion with a 2 cm amplitude at a frequency of 5 Hz.[30] Following the measurements, the signal from a blank cuvette containing only water was recorded and subtracted from the data. The fluorescence spectra were corrected for the sensitivity of the detector and the diffraction efficiency of the gratings in the double monochromator. The excitation energy was varied by a factor of 10 to check for any photointermediate fluorescence.

The 3PEPS and TG spectroscopy was performed with a Coherent Mira-Rega system equipped with an optical parametric amplifier (OPA, Coherent 9450), operating at 60 kHz, using a standard 3PEPS configuration, as shown in Figure 1 (see also e.g., ref 31). The pulse energy was 10 nJ in each beam and the first 2 beams were S-polarized. The polarization of the third beam was rotated by 90° to P-polarization by means of an achromatic waveplate (CVI). In this configuration, the generated 3-pulse echoes have a P-polarization, and can be separated with polarizers from scattering of the first two beams (see e.g., ref 32). To ensure proper alignment and timing, strong echo signals were first generated in a laser dye/solvent system and then spatially filtered. The resulting signals were then sent through cube polarizers and then detected by photodiodes. The zero-delays between the 3 pulses were determined by measuring the 2-pulse echoes for each pulse pair in the laser dye, which are symmetric around zero delay.[33] After this procedure, the flow system was flushed and filled with the protein sample.

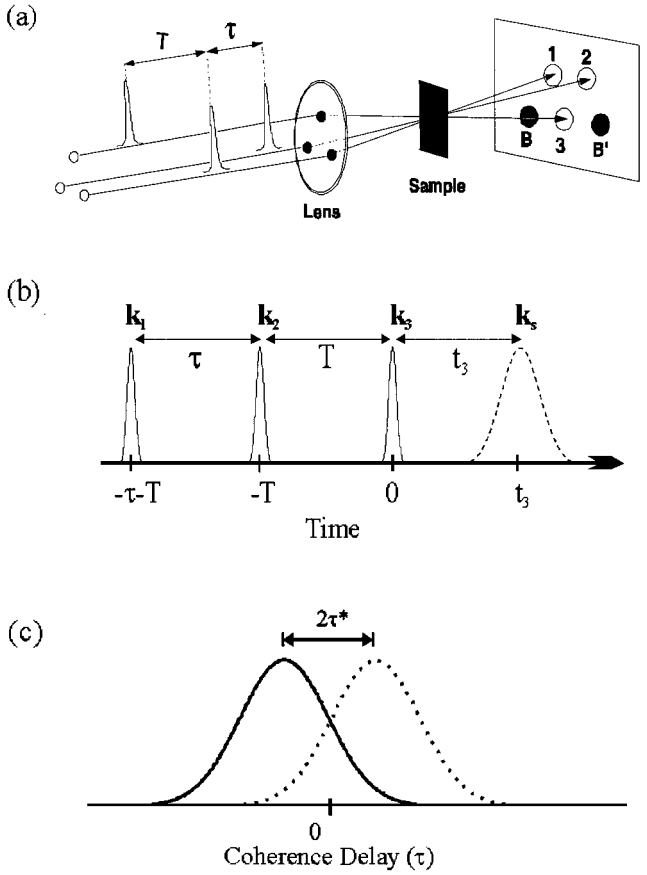

Figure 1. (a) Spatial configuration for the experiments. Three consecutive laser pulses with wave vectors: $\mathbf{k}_1$, $\mathbf{k}_2$, and $\mathbf{k}_3$ are focused in a triangular geometry into the sample. The resulting nonlinear signals are measured along the two phase matched directions $\mathbf{k}_3 + \mathbf{k}_2 - \mathbf{k}_1$ (B) and $\mathbf{k}_3 - \mathbf{k}_2 - \mathbf{k}_1$ (B′). (b) Pulse sequence of the peak shift experiment where the time differences between the three laser pulses, the coherence time, τ, and the population time, T, are experimentally controlled. The echo field generated by the rephasing process is shown by the dotted line. (c). Integrated photon echo traces collected in the B (solid line) and B′ (dashed line) directions at fixed T. The peak shift, τ^*, is half the difference between the signal maxima.

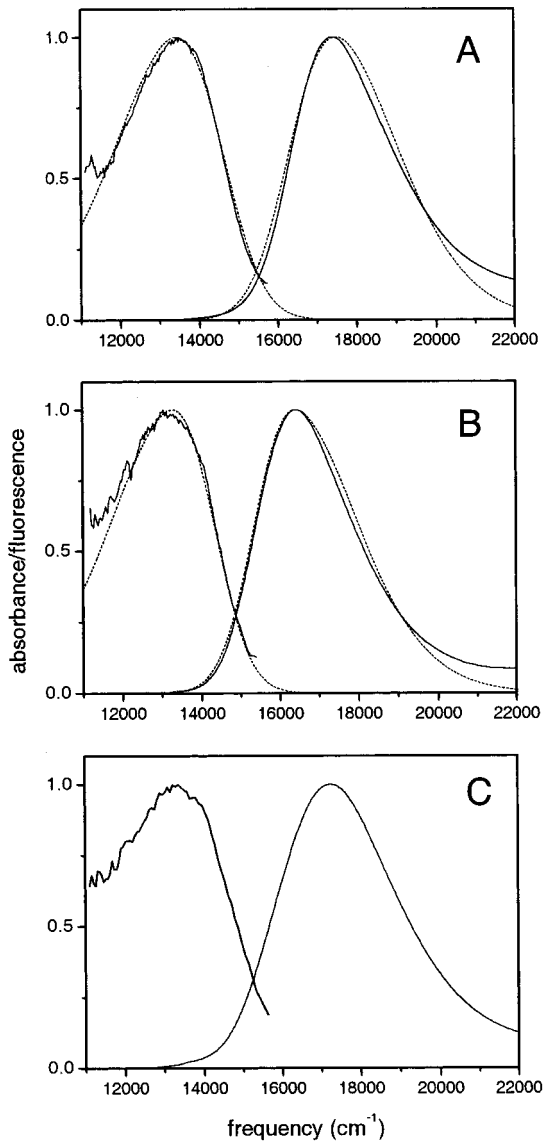

Figure 2. (A) experimental absorption and fluorescence lineshapes of wild-type bacteriorhodopsin (solid lines). The fluorescence spectrum was recorded with excitation light at 550 nm. The dashed lines denote the result of a Multimode Brownian Oscillator (MBO) model simulation. (B) experimental absorption and fluorescence lineshapes of the D85S mutant of bacteriorhodopsin (solid lines). The fluorescence spectrum was recorded with excitation light at 600 nm. The dashed lines denote the result of a MBO model simulation. (C) experimental absorption and fluorescence lineshapes of the D85S mutant of bacteriorhodopsin in the presence of 1 M KCl. The fluorescence spectrum was recorded with excitation light at 550 nm.

The TA spectroscopy was carried out with a home-built amplified Ti:sapphire femtosecond laser system described earlier.[34] The system produced 50 fs pulses at a pulse energy of 15 μJ at 790 nm. The pulses were split and the major part was used to pump an OPA (Coherent 9450), which was tuned to 606 nm and produced pulses with duration of 40 fs after compression in a prism pair. The pump pulses had an energy of 60 nJ and were focused to a spot size of 150 μm. The other part of the amplifier output was focused in a sapphire plate to produce a single-filament white light continuum, which was used as a probe. A long-pass filter or a 0° 800 nm dielectric mirror (CVI) was used to cut out the remaining 790 nm light. Spectral selection took place behind the sample by sending the white light through a monochromator (4 nm bandwidth) after which the light was detected by a photodiode. Unless mentioned otherwise, the pump and probe pulses were polarized parallel. For the anisotropy measurements, the pump was rotated between parallel and perpendicular with an achromatic waveplate (CVI). The instrument response function was determined by measuring the optical Kerr effect of water in the sample cell and could be well represented by a Gaussian with a fwhm of 95 fs. The TA profiles suffered from a contamination with self-phase modulation effects arising from the interaction of pump and probe pulses on the cuvette windows and/or the aqueous buffer, which gave rise to a weak oscillatory feature around zero delay. At 870 nm, the amplitude of this oscillatory feature amounted to ~20% of the signal maximum. This artifact was recorded separately during the same experimental session in the flow system filled with buffer alone. These spurious oscillatory features were directly subtracted from the experimental signals and were largely suppressed in the presented data.

3. Results

3a. Steady-State Spectroscopy. The reorganization energy is a measure of the extent of the chromophore's surroundings' response on optical excitation. It is an important parameter in the quantitative description of excited-state properties of bR and the D85S mutant that we will conduct utilizing the MBO model.

TABLE 1: Spectral Properties

system	absorption line shape peak	absorption line shape fwhm	fluorescence line shape peak	fluorescence line shape fwhm	Stokes shift peak−peak	Stokes shift mean−mean[a]
bR	17 390	3050	13 540	3158	3850	5037
D85S blue form	16 410	2890	13 150	3557/3050[b]	3260	4450
D85S purple form	17 270	3510	13 370	3700	3860	5040

All spectral properties are in units of cm^{-1}. [a] Due to not resolving the complete fluorescence bands, these results are extracted directly from the numerical simulations, which fit the measure fluorescence data (Figure 2). [b] Extracted from simulations as the red edge of fluorescence is poorly resolved.

To determine the reorganization energy of the systems under investigation, steady-state fluorescence measurements on bR and the D85S mutant were performed. Within the harmonic approximation, included in the MBO model, the fluorescence Stokes shift is twice the reorganization energy. Figure 2A shows the absorption and fluorescence spectra of wild-type bR. To enable proper comparison of the shapes of absorption and fluorescence spectra, the spectra are represented as lineshapes (see Appendix). The dashed lines denote the results of a simulation based on a MBO model and will be discussed below. The absorption lineshape has a maximum at 17 390 cm^{-1} (575 nm) and has a full width at half-maximum (fwhm) of 3050 cm^{-1}. The fluorescence lineshape shows a high degree of mirror-symmetry with respect to the absorption spectrum and peaks at 13 540 cm^{-1} (739 nm) with a fwhm of 3158 cm^{-1}. The fluorescence spectrum of wild type bR presented here largely agrees with those in the literature, although there appear to be some variations. It is important to note that the fluorescence spectra and lineshapes cannot be compared directly, as the fluorescence lineshape of bR is shifted to the red by ca. 500 cm^{-1} owing to the $1/\omega^3$ scaling factor applied to the broad fluorescence spectrum. The fluorescence spectrum maxima reported range from 14 300 cm^{-1} (700 nm),[28] 13 700 cm^{-1} (730 nm),[29,35] to 13 300 cm^{-1} (750 nm).[10] Moreover, the latter group reported a fluorescence spectrum which completely lacked mirror symmetry with respect to the absorption.

The lineshapes exhibit a noticeable asymmetry, which results from vibronic contributions. To relate the Stokes shift to the reorganization energy λ, it is in such case appropriate to consider the Stokes shift with respect to the first moments of absorbance and fluorescence lineshapes rather than the maxima, which in fact indicate the mean of the spectra.[6] Considering this, the Stokes shift amounts to 5037 cm^{-1} and the reorganization energy of bR hence is equal to 2518 cm^{-1}. The relevant parameters of the steady-state experiments are summarized in Table 1. As will be shown below, the propagation out of Franck−Condon region is significantly faster than excited-state decay of bR, which implies that very little fluorescence originates from the Franck-Condon region.

The Stokes shift of bR is larger than those of many other photobiological systems. In photosynthetic antennae and reaction centers, the Stokes shift is generally in the order of 10−100 cm^{-1}.[40] However, in photoactive yellow protein (PYP), a bacterial blue-light sensor that exhibits a photocycle similar to that of bR but is structurally completely different, the Stokes shift amounts to ca. 2500 cm^{-1},[37] in the same order of magnitude as bR.

The replacement of the aspartate by a serine in the D85S mutant leads to significant alterations of the functional and spectroscopic properties of the protein. In wild type bR, the carboxyl group of Asp 85 is negatively charged at physiological pH.[1] In the D85S mutant, the serine at this position is neutral, which results in a red shifted absorption spectrum and a deep blue appearance. We refer to this form of the D85S mutant as "blue D85S". As will be shown below, the blue D85S mutant has excited state properties that are dramatically altered with respect to wild-type bR, and are similar to acid blue or deionized bR. Very recently, the atomic structure of the blue D85S mutant has been determined to a resolution of 2.25 Å.[27] The crystal structure indicated that the retinal chromophore assumes an all-trans geometry; however, it could not be excluded that part of the chromophore exists in a 13-cis form.

Upon addition of a concentrated halide solution to the D85S mutant, the absorption spectrum shifts to the blue and the sample color concomitantly changes from blue to purple, resulting in an absorption spectrum that is similar to that of wild type bR. In this purple form of the D85S mutant (hereafter referred to as purple D85S), a halide anion is very likely located at the corresponding position of the carboxyl group of aspartate in wild-type bR. A most remarkable property of the purple D85S mutant is its ability to translocate halide ions toward the cytoplasmic side upon illumination.[38] In this sense, despite a mere 30% sequence homology, it functionally resembles halorhodopsin (hR), the light-driven halide pump which is also found in *Halobacterium salinarum*.[39]

Figure 2B shows the absorption and fluorescence lineshapes of the blue D85S mutant. The absorption is red-shifted and slightly narrowed with respect to wild-type bR. It has an absorption maximum at 16 410 cm^{-1} (609 nm) and a fwhm of 2890 cm^{-1}. The fluorescence peaks at 13 150 cm^{-1} and has a fwhm of 3050 cm^{-1}, and like bR shows mirror symmetry with respect to the absorption. The Stokes shift following from the 1st moments of the absorption and fluorescence spectra amounts to 4450 cm^{-1}. The Stokes shift is significantly smaller, by 579 cm^{-1}, than that of wild-type bR, implying a total reorganization energy of 2225 cm^{-1}. The absorption and fluorescence lineshapes of the blue D85S mutant are simulated utilizing the MBO model (dashed lines).

Figure 2C shows the absorption and fluorescence spectra of the purple D85S mutant in the presence of 1 M KCl. The absorbance lineshape of the purple D85S peaks at 17 270 cm^{-1} (579 nm) and is somewhat broader than that of wild-type bR and the blue D85S mutant, 3510 cm^{-1}, which may originate from a fraction of the sample that has not undergone the blue-to-purple transition. This was confirmed by increasing the KCl concentration to 2M, which led to loss at the red wing of the absorption. On the basis of a spectral deconvolution, we estimate that about 15% of the sample persisted in its native, blue form at 1M KCl (results not shown).

The fluorescence lineshape of the purple D85S mutant is centered at 13370 cm^{-1} (748 nm), and has a width of ca. 3700 cm^{-1}. The fluorescence stokes shift is 5040 cm^{-1}, which is

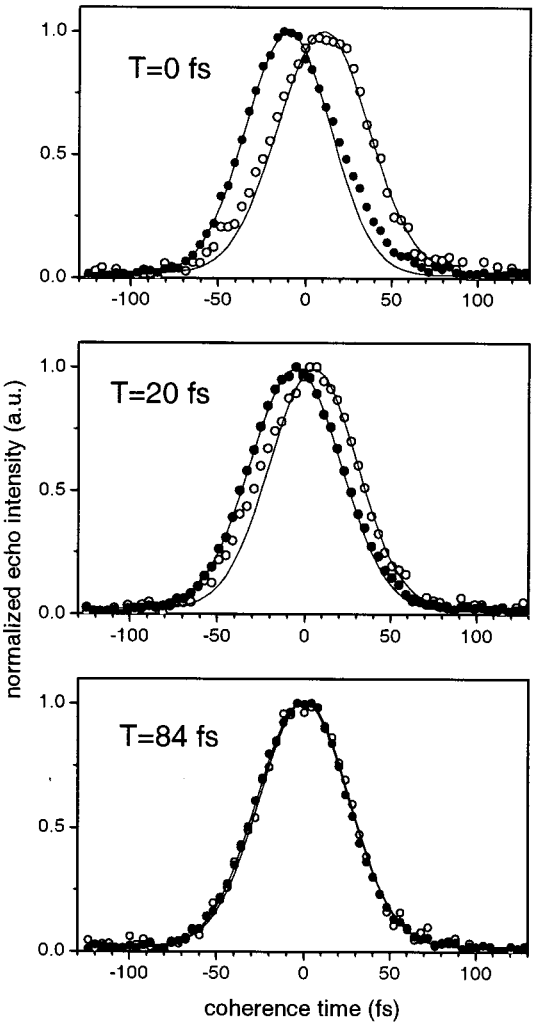

Figure 3. Circles: integrated and normalized 3-pulse echo profiles in the phase matching directions collected at the population times T as indicated in the figures. Solid lines: Gaussian fits to the echo profiles. The 3-pulse echo profiles correspond to peak shift values $t^*(T)$ of 10.5, 3.1, and 0.5 fs, respectively.

increased with respect to the blue D85S mutant but similar to wild-type bR. Because of the heterogeneity in the sample, and the fact that we were not able to collect an extensive femtosecond dataset on this sample, no attempt was made to simulate any data on the purple D85S mutant in the context of the MBO model.

The position of the absorption maximum correlates with the presence of a negative charge at position 85, as noted earlier for the D85T mutant of bR,[40] which shares many spectroscopic and functional properties with the D85S mutant. Importantly, there appears to be a correlation between the presence of a negative charge at position 85 and the size of the reorganization energy. This observation strongly indicates that the protein matrix accounts for a significant portion of the reorganization energy, a point that we will substantiate below.

3b. Time-Resolved Spectroscopy. *Wild-Type bR*. The peak shift, $\tau^*(T)$, at a particular delay T is defined as the shift of the maximum from $\tau = 0$ of the integrated echo signal. As shown previously,[5−7] the measured peak shift profiles are directly related to the transition frequency correlation function, $M(t)$, and hence provide a direct probe of the time scale on which bR loses memory of its original transition frequency. In Figure 3, the integrated and normalized three-pulse photon echo profiles of bR collected at 568 nm (17 600 cm^{-1}) in the phase-matched directions $k_1 - k_2 + k_3$ and $-k_1 + k_2 + k_3$ are depicted. The measured three-pulse photon echo profiles are shown for population times of 0, 20, and 84 fs, with laser pulse durations of 40 fs (Intensity fwhm). Strikingly, the rephasing capability that is present at zero population time has decreased significantly in the echo profiles at 20 fs, and is almost completely lost at 84 fs.

The uncertainties of the peak shift values are estimated at around 500 attoseconds with a 95% confidence level, and were determined by fitting the integrated echo signals to Gaussian functions at long population times and fitting only the positive edges of the echo signals to Gaussian functions at earlier times as shown in Figure 3. Partial Gaussian fitting was applied because the integrated echo signals exhibit a pronounced asymmetry at short population times, and fitting with full Gaussian functions underestimate the magnitude of the peak shift values by up to 3 fs. The asymmetry originates from the different time ordering in the experiment between negative and positive coherence times.[31,50]

The peak shift derived from these three-pulse echo measurements is shown in Figure 4A (circles). The peak shift has an initial value τ_0 of 10.5 fs, and decays rapidly, within 80 fs, to a terminal value of 0.5 fs. After this, no discernible relaxations occur up to a population time of 1 ps. Owing to the short excited-state lifetime of bR (∼500 fs), echo signals at population times longer than 1 ps could not be collected. In Figure 4B, the peak shift profile recorded at 624 nm (16 025 cm^{-1}), which is on the red edge of bR's absorption spectrum, is depicted (circles). It has a initial peak shift τ_0 of 9 fs, which decays within 80 fs to a terminal value of 1 fs.

The 3PEPS profiles shown in Figure 4 on bR have rarely been encountered in 3PEPS spectroscopy. An initial peak shift value of 10.5 or 9 fs is unusually low for dye probe molecules dissolved in organic solvents or polymer glasses, which often exhibit values of 15 to 20 fs.[5,31,36,41] All other pigment−protein complexes studied so far by 3PEPS spectroscopy, i.e., photosynthetic light harvesting antennae[32,42−47] and reaction centers[48] exhibit a large initial peak shift value of about 25 fs. Dye probes bound to the protein lysozyme exhibit an initial peakshift of 16 fs.[49] The low initial peak shift in bR is indicative of a large reorganization energy, consistent with the observed Stokes shift (see Figure 2A).[5]

The rapid decay of the peak shift at 568 nm within 80 fs to 0.5 fs is distinctive. It indicates that bR loses memory of its original transition frequency on this extremely fast time scale. In liquids, multiple components are observed in peak shift decays on time scales of 50 fs to tens of picoseconds, indicative of fast inertial, and slower, diffusive solvation components.[3,5,31] These 3PEPS results thus denote that the diffusive time scale is completely absent in bR's solvation dynamics.

The TG signal for bR measure at 610 nm is displayed in Figure 4C. The initial peak, often referred to as the "coherent spike" or "coherent artifact", accounts for ∼50% of the relaxation of the signals and results from rapid relaxation in the system dynamics upon excitation.[5] In principle, the protein dynamical time scales should be observed in the TG trace, though this may be partially obscured by vibrational contributions, or interference effects between the ground and excited-state responses.[50] In contrast to the 3PEPS signals discussed above, the TG signal also includes decaying components originating from the finite electronic lifetime (Table 2) that makes characterization and separation of these two dynamical processes difficult. As we discuss later, we can accurately simulate the TG traces, with the dynamical information used

TABLE 2: Simulations Parameters

	protein		disorder	vibrations	Stokes shift	excited-state lifetime			
system	$\tau_{g\ (fs)}$	λ_g (cm^{-1})	Δ_{inhomo} (cm^{-1})	$\Sigma\lambda_{vib}$ (cm^{-1})	$2\Sigma\lambda$ (cm^{-1})	a_1 (%)	τ_1	a_2 (%)	τ_2
bR	50	1430	400	1094	5040	77	290 fs	23	1.1 ps
D85S	50	1050	400	1094	4280	65	3.6 ps	35	14 ps

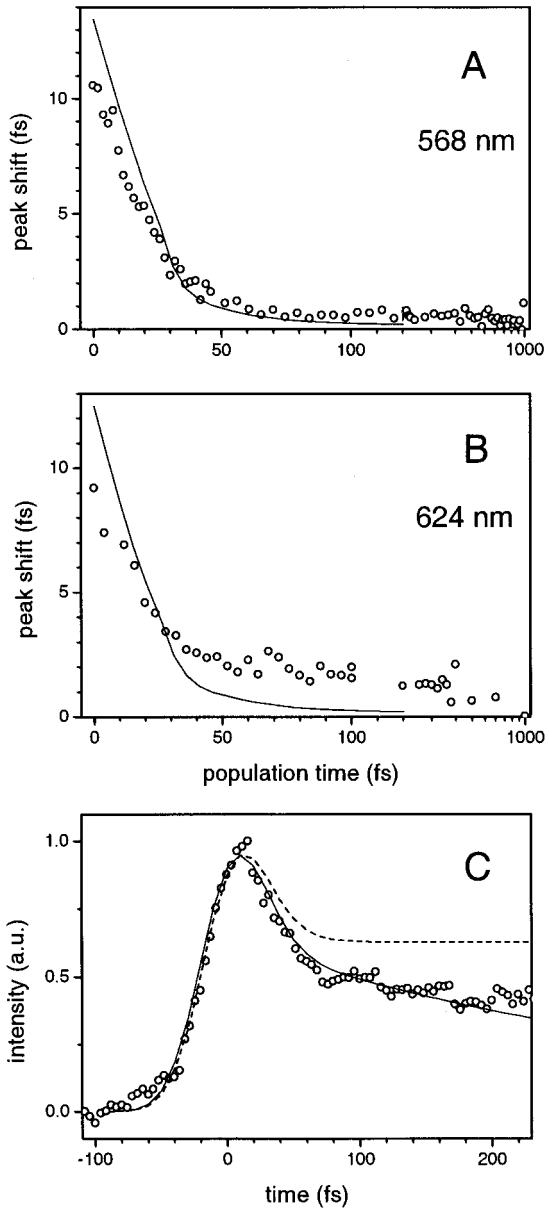

Figure 4. (A) experimental 3PEPS profile for bR taken at 568 nm (circles). Note that the horizontal axis is linear up to 120 fs and logarithmic thereafter; Solid line: simulation with the MBO model with parameters as described in the text. (B) experimental 3PEPS profile for bR at 624 nm (circles). Solid line: MBO simulation (C) transient grating (TG) measurement on bR taken at 610 nm (circles). Solid line: MBO simulation. Dashed line: MBO simulation in the absence of excited-state decay.

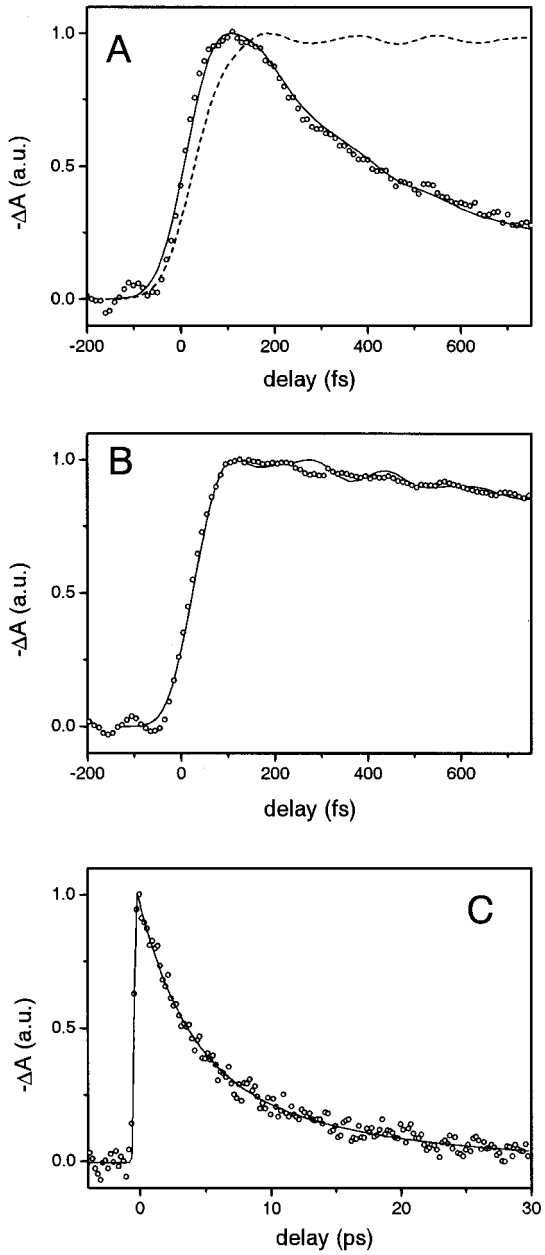

Figure 5. (A) Transient absorption (TA) measurement on bR with excitation at 606 nm and probe at 870 nm (circles). The solid line denotes the result of the MBO simulation described in the text. Dashed line: simulated curve in the absence of excited-state decay. (B) TA measurement on the D85S mutant of bR with excitation at 606 nm and probe at 870 nm (circles). The solid line denotes a simulation with the MBO model with parameters as described in the text. (C) TA measurement on the blue D85S mutant with excitation at 606 nm and probe at 856 nm (circles) on a 30 ps time axis. The solid line line denotes a biexponential fit with time constants of 3.5 ps (65%) and 15 ps (35%).

to simulate the 3PEPS and TA measurements, which provides for a check on the self-consistency of the measurements and the numerical calculations.

To complement the 3PEPS and TG measurements shown in Figure 4A, B, C, and facilitate comparison with the results of other groups,[22−24,51] TA measurements have been performed. Figure 5A shows the kinetics in bR probed at 870 nm (11495 cm^{-1}) upon excitation at 606 nm (16500 cm^{-1}). At this wavelength, stimulated emission from the excited state to the ground state at the far red edge of the emission spectrum is observed (see Figure 2A), and thus the dynamic Stokes shift is monitored. The instrument response function, determined by measuring the optical Kerr effect in water has a Gaussian shape with a fwhm of 95 fs. The TA signal at 870 nm shows a rapid

rise of the stimulated emission, followed by a decay on a time scale of a few hundreds of fs. A biexponential fit convoluted with a Gaussian instrument response to the data (not shown) yielded excited-state lifetimes of 290 fs (78%) and 1 ps (22%), in good agreement with earlier results.[13,22] The shape of the TA signal during the first ~200 fs looks unusual in the sense that it exhibits a rather broad and symmetric peak around the maximum at 120 fs and is poorly described by exponential functions. Moreover, weak oscillations can be discerned which appear to persist on a picosecond time scale. Although the self-modulation artifact certainly disturbs the signal to some extent, as evidenced by the small oscillations before zero which arise from an incomplete subtraction, it is too small and limited in time to give rise to the nonexponential behavior.

The phenomenon that the stimulated emission from bR rises very rapidly is consistent with the rapid decay of the peak shift shown in Figure 4A and B. The rapid rise has been well documented in earlier fluorescence upconversion[13] and TA studies[22−24] and has been the main rationale for a revision of the two-state model originally proposed by Zinth[10] and Mathies and co-workers.[11]

Blue D85S Mutant. The D85S mutant has a dramatic increase of its excited-state lifetime as compared to wild-type bR. This is illustrated in Figure 5C, which shows the TA signal on a 30 ps time axis, with excitation at 606 nm (16 500 cm^{-1}) and probing at 856 nm (11 680 cm^{-1}) at the red edge of stimulated emission. A biexponential fit of this trace indicates lifetimes of 3.5 ps (65%) and 14 ps (35%), which is expected from earlier results on acid or deionized blue bR and the D85N mutant.[19] TA experiments probed at 480 nm, where the signals are dominated by a strong excited-state absorption, and at 660 nm, where a K-like intermediate absorbs, gave similar time constants. In the spectral region around 750 nm (13 330 cm^{-1}) there was little signal in the D85S mutant at all times, indicating that stimulated emission and excited-state absorption cancel, similar to the situation in wild-type bR (results not shown,[22,23]).

Figure 5B shows the short-time dynamics at 870 nm (11 495 cm^{-1}). A rapid rise of the stimulated emission is observed. In contrast to wild type bR, the stimulated emission hardly decays during the first picosecond as a result of the increased excited-state lifetime. As with wild-type bR, we observe weak oscillatory features in the stimulated emission. It is an important observation that within the excited-state lifetime of 3.5 ps, no slower rise terms on time scales of >100 fs components are observed. It could be argued that in wild-type bR, evolution of the stimulated emission due to "diffusive"-type protein solvation components on a sub-ps to ps time scale could go unnoticed owing to bR's short excited-state lifetime of 290 fs. The blue D85S mutant provides for an extended detection window because of the increased lifetime, and any such evolution would be revealed. However, no slow rise components are observed, which indicates that reorganization in the D85S mutant of bR does not occur on time scales longer than 100 fs.

We conclude that our 3PEPS, TG, and TA measurements on wild-type bR and the blue D85S mutant shown in Figures 4 and 5 exhibit the same trend: after ~80 fs, the reorganization is essentially complete. It is important to note that such is certainly not the case for all-trans retinal in solution: TA studies have clearly demonstrated that stimulated emission shows spectral shifting on a sub-ps to ps time scale in this circumstance.[52,53]

3c. Modeling of Static and Time-Resolved Data. One of the goals of our study is to characterize and separate the dynamics originating from the excitation of the intramolecular vibrations of retinal from the intermolecular relaxation of the protein environment. To accomplish this, the collected spectroscopic signals were analyzed with the use of the multi-mode Brownian oscillator (MBO) formalism with an explicit inclusion of the intramolecular degrees of freedom to describe both linear and nonlinear signals in terms of the underlying dynamical processes. A full description of this method can be found in ref 50, a brief account relevant to the present experimental data is given in the Appendix.

Our approach is similar to that taken by Wexler et al. to describe steady-state and TA data on wild-type bR.[29] However, in our study we also consider the unique results of 3PEPS and TG spectroscopy and data from the D85S mutant. We simulated the red edge of stimulated emission near 870 nm, which was not considered by Wexler et al. The TA signals around 870 nm are not contaminated by excited-state absorption, leading to a number of recent studies of this wavelength region.[22−24,51] Thus, a comparison with the results of our simulations should be highly relevant.

The frequencies and displacements of the intramolecular vibrations of retinal in bR in the ground state have been determined by Mathies and co-workers.[54] The intramolecular modes account for 1094 cm^{-1} of reorganization energy, requiring a significant contribution of the protein dynamics to the observed 5040 cm^{-1} Stokes shift. We conclude that a significant protein solvation component of about 1400 cm^{-1} is needed. This protein solvation component must show a very fast relaxation, as indicated by the ultrafast decay of the 3PEPS trace and the rise of the stimulated emission. In analogy with solvation dynamics in liquids, such fast relaxations are very likely the result of "inertial" solvent or protein motions, and are usually described by a Gaussian decay component.[3] We therefore attempt to describe bR's lineshapes and nonlinear spectroscopic features with a minimal two-component model, consisting of the intramolecular modes and a Gaussian relaxation of the protein with a λ of 1430 cm^{-1}, and a width of 50 fs. Furthermore, an inhomogeneous broadening of 400 cm^{-1} (fwhm) is assumed. The result is shown as the dashed lines in the absorption and fluorescence lineshapes in Figure 2, and the solid lines in the 3PEPS measurements of Figure 4A and B, the solid line in the TG measurement in Figure 4C and the solid line in the TA measurement of Figure 5A.

The absorption and fluorescence lineshapes in Figure 2A are reasonably described by these parameters: the fluorescence Stokes shift is reproduced, and the widths and shapes of the simulated spectra match. The vibronic feature near 18 000 cm^{-1} is slightly overestimated by the simulation, as is the red edge of the absorption lineshape. We attempted to simulate the lineshapes with the relative contribution by the intramolecular displacements scaled up or down, but we found that there was little freedom in doing so; an increase of the displacements by 30% led to clearly too much vibronic structure on the absorption lineshape. A decrease of the displacements by the same amount, while increasing the Gaussian component to maintain the fluorescence Stokes shift, resulted in lineshapes that were too symmetric.

In Figure 4A, the solid line shows the simulated peak shift calculated for 568 nm (17 600 cm^{-1}). The simulated initial peak shift amounts to 13.5 fs, somewhat higher than the experimental value of 10.5 fs. This difference is actually acceptable, considering that experimental initial peak shifts generally tend to be lower than in the simulations. It was recently shown that this probably results from slight chirping of the femtosecond pulses, which commonly occurs in the laboratory.[50] The simulated peak

shift profile has a bimodal character: the first 30 fs of the simulated peak shift decay to about 2.5 fs can be related to destructive interference between the high-frequency intramolecular modes of retinal. Similar observations were made in the laser dye Nile Blue in acetonitrile, which exhibits mode displacements similar to retinal.[31,50] The further peak shift decay from 3 to 0.2 fs is slower, occurring from 30 to 100 fs, and follows from the Gaussian protein solvation contribution. The agreement between experiment and simulation is actually very good for these population times.

In Figure 4B, the calculated peak shift at 624 nm (16 025 cm^{-1}), at the red edge of the absorption is shown. It is very similar to that simulated for 568 nm with an initial peak shift τ_0 of 12.5 fs, and a rapid decay to a terminal peak shift of 0.2 fs. The simulation at 624 nm deviates more strongly from the experimental data than that at 568 nm: the experimental peak shift starts lower, at 9 fs, and has a higher terminal value of 1 fs. A possible explanation for the discrepancy is the presence of a significant excited-state absorption of bR at this wavelength, which has a magnitude comparable to the ground-state absorption,[22] as numerical calculations of Xu et al. have indicated that interference effects resulting from excited state absorption may lead to a decreased experimentally observed initial peak shift and an increased terminal peak shift.[55] It was recently shown that in 3PEPS spectroscopy, the solvation component gains amplitude with respect to the destructive interference effect of the intramolecular modes when a peak shift is recorded at the red edge of the absorption band rather than the absorption maximum,[36] and in this sense the anomalous behavior of the peak shift at 624 nm is unfortunate. Nevertheless, the agreement between 3PEPS experiments and simulations at 568 nm clearly shows that the MBO model accounts for the essential features of solvation dynamics in bR.

The numerical simulations of the TG signals, including both excited state lifetime effects (solid line) and solely the solvation response (dashed line) are presented with the experimental data (circles) in Figure 4C. As is illustrated, to get satisfactory agreement between the simulations and the experimental data, the excited state lifetime must be convolved into the bare solvation response from the protein (and vibrations). The 300 fs decay observed on the shoulder of the coherent artifact of the experimental data is probably not the result of solvation dynamics, but rather of the lifetime effects: Otherwise, this decay component would be observed in the 3PEPS data, although the rapid peak shift decay resulting from the vibronic contribution might partly obscure such a component. The fact that we can accurately simulate both the TG and the 3PEPS signals with a single set of parameters adds confidence to our analysis of the experimental data with the MBO model.

The simulation carried out on the basis of the above-described two-component model for the TA signal in bR is depicted in Figure 5A. A biphasic excited state population decay of 290 fs and 1 ps was assumed. The simulated signal rises fast, and reaches a maximum at 100 fs. Strikingly, the nonexponential shape of the TA signal at early times is well reproduced, and shows that it is actually due to the combination of a short excited state lifetime and the presence of excited state oscillations. The simulated curve exhibits slight further oscillatory features that coincide with the experimental curve. In the simulations, the oscillations arise from wave packet motion of impulsively excited low-frequency intramolecular vibrations. The dominant low-frequency mode of retinal has a frequency of 189 cm^{-1}, with a displacement of 0.85. The 189 cm^{-1} vibrational mode was phase-shifted by π (the phase factor was added in the argument of the exponential function in eq 6 of the Appendix), which resulted in a compelling agreement with the experiment. A possible explanation for the occurrence of the phase shift follows from recent work by Kobayashi et al., who observed a strong time-dependence of retinal's mode frequencies. More specifically, the C=C−H in plane mode (1150−1250-cm^{-1}) and hydrogen out of plane modes (900−1000 cm^{-1}) merged into a single frequency and then separated again after 170 fs,[25] indicating significant skeletal stretching and twisting of the chromophore. Possibly, these motions put energy into the low frequency mode of retinal and produce the phase shift. The calculated results indicate that the experimentally observed oscillations exclusively result from retinal's intramolecular vibrational structure, and not from vibronic coupling with protein modes, as is the case in many photosynthetic proteins.[56,57]

In Figure 5A, the simulated TA signal in the absence of excited state decay is plotted as well (dashed line). The rise of the signal is significantly slower than with the finite lifetime and reaches its maximum at 180 fs. The actual apparent faster rise time in bR with respect to this latter curve is an effect that results from the combined actions of a noninstantaneous rise and the onset of the 290 fs electronic lifetime decay component. This effect has not been realized before and the failure to resolve the dynamic Stokes shift by many authors may be traced back to this phenomenon.

We have also simulated the experimental results on the blue D85S mutant in the context of the MBO model, and the results are shown in Figure 2B for the absorption and fluorescence lineshapes (dashed lines) and the TA data in Figure 5B (solid line). The displacements of the intramolecular vibrations of retinal were kept the same as in wild-type bR, but the reorganization energy of the Gaussian protein solvation component was reduced by 370 cm^{-1} to match the significantly smaller Stokes shift of the fluorescence and the slightly narrower width of the absorption. The excited-state lifetimes were fixed to 3.5 and 14 ps. The fast rise of the stimulated emission is well described by the MBO simulation. However, the oscillatory pattern is not as well reproduced as for wild type bR. Nevertheless, we conclude that a minimal model, by which we only assume a 50 fs Gaussian relaxation component for the protein, and the known intramolecular vibrations of the retinal chromophore, is sufficient to reproduce the essential properties of the linear and nonlinear signals in bR and the blue D85S mutant.

The dynamic aspects of the stimulated emission in bR have been under intense scrutiny by several research groups, and it is of interest to test whether the outcome of the MBO model is consistent with these experimental results. Ruhman and co-workers have monitored the stimulated emission of bR and of modified bR with a locked retinal chromophore at 800 nm (12 500 cm^{-1}) and 950 nm (10 525 cm^{-1}) with a time resolution of 30 fs.[24] In modified bR, the locked retinal chromophore is unable to isomerize, and as a consequence its excited-state lifetime is increased to ~10 ps. Figure 6 shows the results of the MBO model, with the same parameters for wild-type bR as summarized in Table 2, but with a shorter instrument response function of 30 fs intensity fwhm and an infinite excited-state lifetime for modified (locked) bR. Figure 6A shows the results for native bR for 800 nm (solid line) and 950 nm (dashed line). Ruhman and co-workers observed an oscillatory signal with a dominant mode at 150 cm^{-1}, which likely corresponds to the highly displaced 189 cm^{-1} mode in the resonance Raman spectrum of bR.[54] Moreover, the stimulated emission at 950 nm lagged that at 800 nm by 10−20 fs. As indicated in Figure 6A, the oscillatory features and the lag of stimulated emission

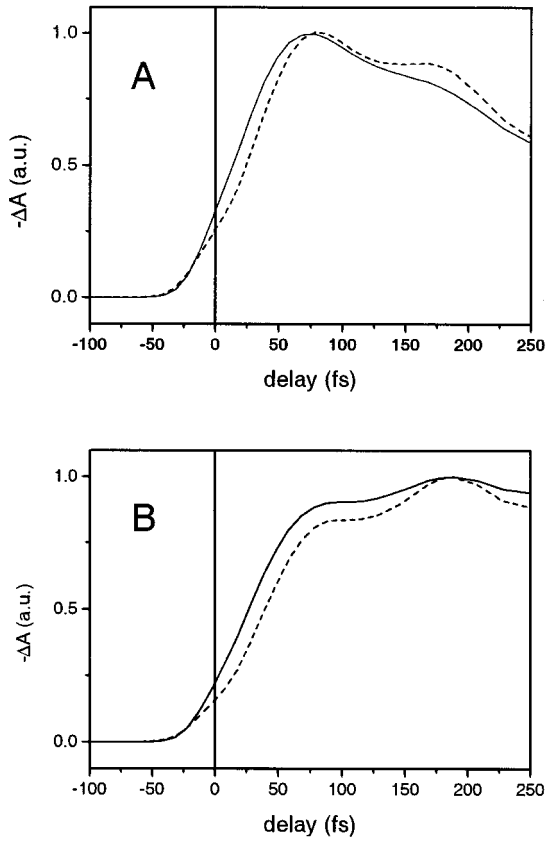

Figure 6. (A) Result of MBO simulation of TA measurement on native bR, with excitation at 606 nm and probe at 800 nm (solid line) and 950 nm (dashed line), with a 30 fs instrument response function and further parameters as described in Table 2 and in the text. (B) result of MBO simulation of TA measurement on modified bR with a locked chromophore, with excitation at 606 nm and probe at 800 nm (solid line) and 950 nm (dashed line). with a 30 fs instrument response function and further parameters as described in Table 2 and in the text.

at 950 nm are reproduced by the MBO model, although the simulated lag appears to be somewhat underestimated. Interestingly, in the context of the MBO model, the lag of the stimulated emission at 950 nm does not result from the Gaussian relaxation component, but solely from phase differences in the oscillatory features resulting from coherent wave packet motion, which arise from probing at different displacements in the potential well: when only a Gaussian relaxation was assumed without coupling to intramolecular vibrational modes, the traces at 800 and 950 nm became indistinguishable.

Figure 6B shows the simulated results for modified bR with the locked chromophore, with stimulated emission probed at 800 nm (solid line) and 950 nm (dashed line). As for native bR, the experimental results indicated oscillatory features and a lag of stimulated emission at 950 nm, which are well reproduced by the MBO simulation. Ruhman and co-workers reported a "slow" rising component of 100−200 fs in modified bR, which was absent in native bR. As shown in Figure 6B, this feature is well reproduced in the MBO simulation, and results from its increased excited-state lifetime (as discussed above), combined with the effects of excited-state oscillations.

Zinth and co-workers have conducted a TA study with a time resolution of <20 fs, and observed a high-frequency oscillation at 770 cm^{-1}, which was even apparent in the rise of the stimulated emission.[51] The latter mode does not correspond to any highly displaced mode of the resonant Raman spectrum of bR, and may arise from a frequency shift of one of the dominant

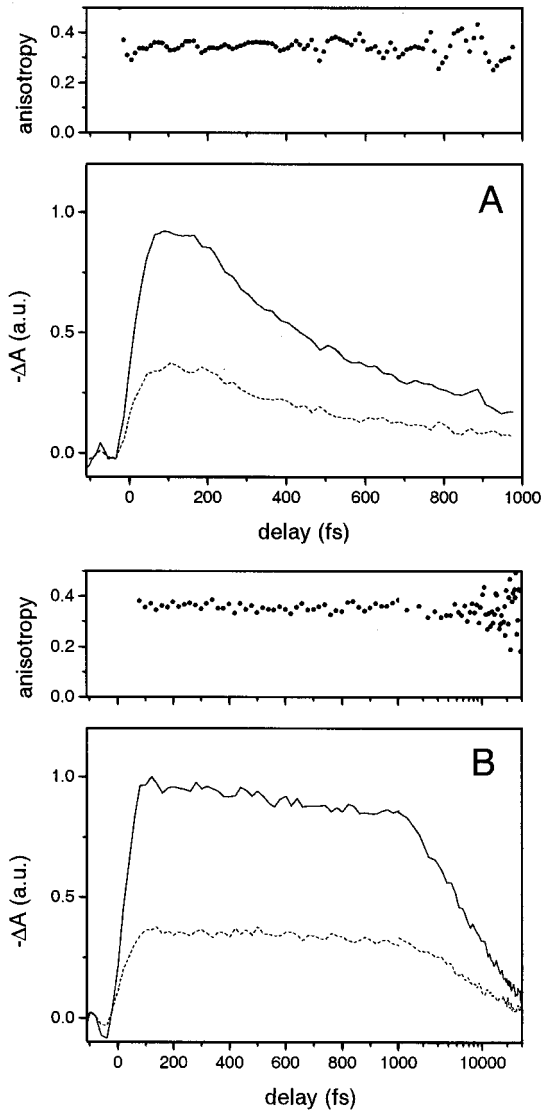

Figure 7. (A) TA measurement on wild-type bR with excitation at 606 nm and detection at 886 nm, with pump and probe beams polarized parallel (solid line) and perpendicular (dashed line). The dotted line denotes the anisotropy. (B) TA measurement on the D85S mutant of bR with excitation at 606 nm and detection at 886 nm, with pump and probe beams polarized parallel (solid line) and perpendicular (dashed line). The dotted line denotes the anisotropy. Note that the time axis is linear up to 1 ps and logarithmic thereafter.

high-frequency modes upon excitation. Such shifts have very recently been observed by Kobayashi et al..[25] Moreover, hole-burning spectroscopy has indicated that the dominant C=C stretch mode at 1527 cm^{-1} in bR shifts down to 1250−1450 cm^{-1} in the excited state.[58] An alternate explanation of the 770 cm^{-1} oscillation's origin may result from an interference between the 1008 cm^{-1} and the 266 cm^{-1} vibrational modes[54] that will generate an oscillating component[36] with a difference frequency of 742 cm^{-1}.

3d. Time-Dependent Anisotropy of the Stimulated Emission. It has been proposed that retinal undergoes a rapid torsional motion after photoexcitation and assumes a 90° twisted form about the C_{13}=C_{14} double bond after ~200 fs.[10−12,21] This putative state, which is an excited-state species, is sometimes referred to as I_{460}. To test this idea, we have undertaken a time-resolved anisotropy study of the stimulated emission in bR and the blue D85S mutant. In Figure 7A, the kinetics of wild-type bR probed at 886 nm (11285 cm^{-1}) with pump and probe

polarized parallel (solid line) and perpendicular (dotted line) are plotted, together with the anisotropy calculated from these kinetics. The excitation wavelength was 606 nm (16 500 cm^{-1}). At 886 nm, contributions from excited-state absorption are negligible,[22] and consequently, this measurement provides for a reliable probe of orientational changes of retinal's transition dipole moment in the excited state. The anisotropy has a value of 0.35, close the theoretical maximum of 0.4 for the initially prepared excitation on the chromophore, and does not show any time dependence during the excited-state lifetime of bR. A similar measurement probed at 928 nm (10 775 cm^{-1}) gave identical results (not shown). Fluorescence upconversion measurements of Du and Fleming showed a time-independent anisotropy of 0.26 near 886 nm.[13] The reason for this discrepancy is unclear, but with the high time resolution of Du and Fleming (60 fs) it is unlikely that anisotropy decay could have occurred within their instrument response. Figure 7B shows the corresponding data for the D85S mutant. Note that the scale is linear up to 1 ps, and logarithmic thereafter. As in wild type bR, the anisotropy has a time-independent value of 0.35. These results indicate that during the respective excited state lifetimes of wild type bR and the D85S mutant, no change of the direction of the retinal chromophore's transition dipole moment takes place. It is therefore highly unlikely that I_{460} corresponds to a species with a 90° twist about the C_{13}=C_{14} double bond. We note that the occurrence of such a conformation would be doubtful on the sub-ps time scale because the covalent cysteine linkage to the protein would restrain it. It cannot be excluded, however, that on this time scale, retinal is seriously twisted and stretched in a way that the transition dipole moment is not changed appreciably.

3e. Time-Resolved Spectroscopy of the Purple D85S Mutant. We conclude the results section by presenting our femtosecond measurements on the purple D85S mutant. Unfortunately, in the presence of high halide concentrations, the purple D85S protein bleached and aggregated quickly upon exposure to femtosecond laser pulses, which precluded the collection of an extensive dataset on this sample.

Figure 8A shows the kinetic trace probed at 480 nm in the purple D85S mutant upon excitation at 606 nm. A pronounced excited state absorption is located at 480 nm, and this measurement interrogates the excited state lifetime. The trace can be well fitted with a biexponential function with time constants of 620 fs (60%) and 3.5 ps (40%). This indicates that the purple D85S mutant has a decreased excited state lifetime with respect to its native, blue form, and is comparable to that of wild type bR (Table 2). We note that the 3.5 ps component may at least partly be caused by a fraction of protein that persists in its blue form (see section 4a). It thus appears that the presence of a negative charge at position 85 catalyzes the primary photochemistry. This phenomenon was reported earlier by Logunov et al.,[59] who observed that addition of chloride ions to the D85N mutant led to a lifetime decrease from 5 to 0.5 ps. The excited-state lifetime of the purple D85S mutant is shorter than those reported for the light-driven halide pump hR, where a single lifetime of 3 ps[60] and biexponential lifetimes of 1.5 and 8 ps[61] have been reported.

Figure 8B shows the evolution of the stimulated emission probed at 928 nm of purple D85S upon excitation at 606 nm (solid line). For comparison, the corresponding signal in wild type bR is also shown (dashed line). The rise of the stimulated emission is essentially the same, whereas its decay is somewhat slower in purple D85S, which is expected on the basis of its slightly longer excited state lifetime. The similarities between

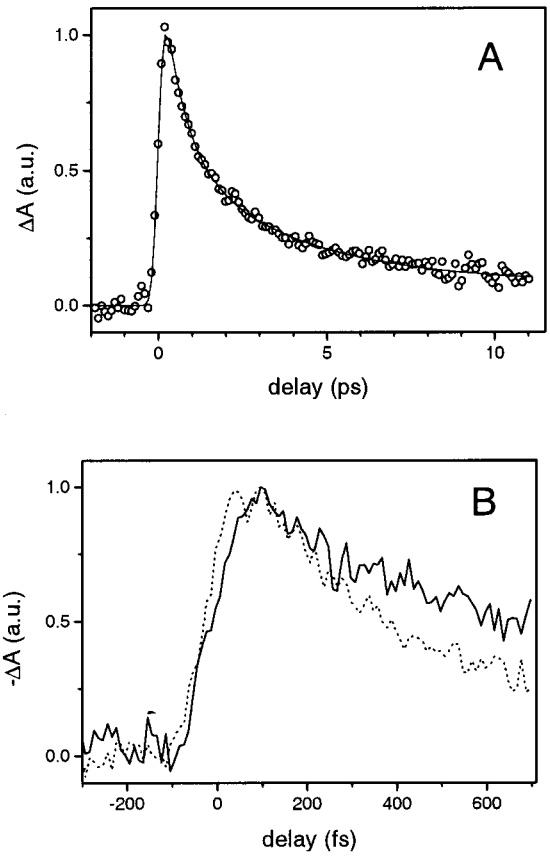

Figure 8. (A) TA measurement on the purple D85S mutant of bR in the presence of 1 M KCl with excitation at 606 nm and detection at 480 nm (circles). The solid line denotes a two-component fit to the experimental data with time constants of 620 fs (60%) and 3.5 ps (40%). (B) TA measurement on the D85S mutant of bR in the presence of 1 M KCl (solid line) and wild-type bR (dashed line) with excitation at 606 nm and detection at 928 nm.

bR and purple D85S, in steady-state as well as nonlinear experiments indicate that the conclusions that are drawn in this paper regarding the nature of excited state relaxations in bR are very likely valid for purple D85S too.

4. Discussion

In this work, the dynamic aspects of the reorganization of bR and its D85S mutant after photoexcitation were studied with linear and nonlinear spectroscopy. The results were described in the context of the multimode Brownian oscillator model. It was concluded that the time-resolved and steady-state data can satisfactorily be described with a surprisingly simple model that encompasses known couplings to intramolecular vibrations of the retinal chromophore with a contribution of 1100 cm^{-1} to the reorganization energy, and a single, Gaussian protein relaxation component which represents 1430 cm^{-1} of reorganization energy. In the D85S mutant of bR, where a charged amino acid near the retinal chromophore has been replaced by a neutral one, the magnitude of the Gaussian component is diminished by 380 cm^{-1} to 1050 cm^{-1}.

To date, few studies have addressed the issue of protein dynamics after creating an excited state on protein-bound chromophores. Jordanides et al. have performed a 3PEPS study of the dye eosin bound to lysozyme. They concluded that the main properties of this system were dictated by the exposure of eosin to water molecules, be it in the solvent or bound to the protein.[49] Beck and co-workers investigated the photosynthetic

light harvesting complex allophycocyanin, and found that 90% of the solvation of bilin chromophores in the protein matrix occurred within 100 fs.[44] Hochstrasser and co-workers have reported a TA study on coumarin bound to calmodulin, where they observed a major fast solvation, along with a minor slow solvation component on a ~1 ps time scale.[62] All these systems qualitatively exhibit dynamics similar to bR, although they all exhibit minor slow, diffusive components. They differ greatly, however, in the size of the reorganization energy, which is in all cases much smaller than in bR. It must be noted that all these systems are nonreactive, and that the protein exerts an entirely different function, or has no light-activated function at all.

The Gaussian component can, in analogy with solvation dynamics in liquids, be related to inertial motions, i.e., small scale, free and unrestricted motions of the individual groups of the protein scaffolding in the potential wells which they occupied before optical excitation. Our results strongly indicate that after the Gaussian, inertial relaxation, no diffusion-type motions take place up to a few ps in bR. The absence of such diffusive motion is very likely due to the covalently constrained, polymeric nature of the protein.

Schulten and co-workers have studied the early light-induced events in bR by structure-based MD simulations.[63] The retinal chromophore in bR exhibits a very large difference dipole of 13.5 D on optical excitation, corresponding to the transfer of almost a quarter of an elementary charge toward the Schiff base terminus.[64,65] Schulten and co-workers have taken into account this property, and found that upon such a charge redistribution, the protein shows an extensive dielectric relaxation with a magnitude of ~1700 cm^{-1}, which occurs on a time scale of 100 fs. This result is in striking quantitative agreement with our findings, and it may be concluded that the large Gaussian component in the reorganization energy in bR is mainly, if not entirely, the result of the unusually large charge-transfer character of retinal's excited state. The good agreement lends credence to Xu and Schulten's viewpoint that the ultrafast relaxation is dielectric in nature. The simulations on bR and MD simulations on electron-transfer reactions in photosynthetic reaction centers[66,67] showed that the relaxations involve relatively small motions of many nuclei up to relatively long distances from the chromophore. The protein conformation was distorted only minimally due to large activation barriers, in agreement with our finding that "diffusive" protein relaxations do not occur.

We conclude that on the sub-ps to ps timescale, on which the isomerization of retinal takes place, the protein's major energetic influence is electrostatic via a large number of small amplitude motions of charges and dipoles. Major structural rearrangement of the protein that might, for example, direct the reactive motion by repulsive interactions, do not occur on the timescale of the isomerization.

It was suggested by Schulten and co-workers that the collective dielectric response of the protein could be coupled to coherent wave packet motion on retinal. In this respect, the ultrafast stretching and twisting of retinal on a <1 ps time scale, observed recently by Kobayashi et al. with sub-5 fs spectroscopy,[25] might, at least in part, proceed under the influence of the dielectric response of the protein. Furthermore, the protein's dielectric response could effectively distort the excited-state energy potential energy surface in such a way that the coupling with the ground state, and thus the rate of internal conversion, is enhanced. In these ways, the dielectric response of the protein may become part of the isomerization reaction coordinate.[63]

The excited state dynamics in bR as probed by TA spectroscopy have previously been described in terms of evolution along isomerization reaction coordinates, especially torsional and stretching degrees of freedom of the retinal chromophore.[10,11,22−24] These experiments have provided the main experimental support for the two most widely accepted reaction mechanisms, the two-state model[10,11] and the three-state model.[22,23,68] Our finding that a broad collection of linear and nonlinear spectroscopic measurements on bR and the D85S mutant can be well described with a model that only considers a Gaussian protein relaxation indicates that these spectroscopic techniques may in fact not be very sensitive to the reaction-coupled structural changes in the retinal chromophore that take place as the system evolves on its potential energy surface. Very recently, TA spectroscopy with extremely short pulses has revealed dynamic changes in retinal's vibrational structure in real time.[25] Such time-resolved vibrational techniques, which include time-resolved resonant Raman[16] and coherent anti-Stokes Raman spectroscopy,[14,17] and time-resolved X-ray crystallography[69] may prove more incisive in deciding on the mechanistic aspects of bR's photoisomerization reaction.

The question remains as of what property of the protein catalyzes bR's isomerization reaction, having established that the protein exhibits no appreciable structural reorganization after retinal photoexcitation. Apart from the above notions concerning the role of the dielectric relaxation of the protein, we indicate a possible role for the protein's diffusive fluctuations that exist in the *ground state* of bR, and are not altered on photoexcitation, which may control the photoisomerization of retinal. The bond lengths of retinal change significantly upon excitation,[20,25] which indicates that the rigidity of its polyene backbone may decrease after excitation. It is conceivable that large-scale, diffusive protein fluctuations have no effect on a rigid retinal chromophore in its ground state, but may force retinal to its 13-cis form when it has an increased flexibility in the excited state. A requirement for the occurrence of such process would be that the 13-cis isomer of retinal would "fit well" into the protein binding pocket. In this scenario, photoisomerization of retinal does not create a steric conflict in the binding pocket, which is often presumed to be a driving force for conformational changes in the protein.[16,70,71] Instead, retinal isomerization would rather serve to disrupt the hydrogen bonding network around retinal, which in turn could lead to functional structural changes in the protein. It is interesting to note that dark-adapted bR contains an evenly distributed mixture of all-trans and 13-cis, 15-anti retinal, which indicates that there is virtually no change in free energy in bR for these isomers of retinal. In light of these considerations, it is of interest to allude to the recent results of MD simulations on the bacterial blue-light receptor PYP. Like bR, the photochemistry of PYP involves a trans-cis isomerization of its chromophore, *in casu* a p-coumaric acid, around a C═C double bond. It was shown that large-scale, concerted, so-called "essential" motions exist in the protein, and that some of these motions occur in the immediate vicinity of the chromophore.[72] When emulating the excited state of the p-coumaric acid chromophore by removing the double bond potential, it was found that on a picosecond time scale, isomerization of the chromophore took place as a result of the interaction with the protein's large scale motions.

Acknowledgment. The authors acknowledge Professor J. Lanyi for the gift of the D85S mutant and a wild type bR sample. Great thanks goes to Dr. Mino Yang (University of California, Berkeley) and Prof. Taiha Joo (POSTECH University, Korea) for useful advice on conducting the MBO simulations. JK is

grateful to the Human Frontier Science Program Organization (HFSPO) for granting a long-term fellowship. K.O. is a Japan Society for the Promotion of Science (JSPS) Research Fellow. This work was supported, in part, by a grant to G.R.F. from the National Science Foundation, and by the NIH, P01 GM51487 (R.M.G.).

5. Appendix: Theoretical Methods

To quantitatively account for the excited-state properties of bR as probed by the various linear and nonlinear spectroscopies applied in this study, the data are described in the framework of the multimode Brownian oscillator (MBO) model, formalized by Mukamel and co-workers.[73] The application of the MBO model for analyzing our data allows for a quantitative investigation of the dynamical interactions between the retinal chromophore and its protein surroundings (including vibrational effects) following photoexcitation. Several discussions of the MBO model as it applies to third-order nonlinear optical signals have been described elsewhere in detail,[5,6,50,73] however, we briefly outline of the relevant features of the model to aid in the presentation and interpretation of our experimental data.

The transition frequency between the ground and excited electronic states of an embedded chromophore in a condensed phase is not static, but varies in time as it interacts (e.g., collides) with the molecules in the surrounding environment. In the case of the retinal chromophore in bR, these interactions are with the residues of the surrounding protein and with water molecules trapped within the protein matrix. Subsequently, for an individual chromophore, *i,* the transition frequency can be separated into three components

$$\omega^i_{eg}(t) = \langle\omega_{eg}\rangle + \delta\omega^i_{eg}(t) + \epsilon_i \tag{1}$$

where $\langle\omega_{eg}\rangle$ is the average value of the transition frequency, $\delta\omega^i_{eg}(t)$is the fluctuating part of the electronic transition frequency (induced by the interactions with the surroundings), and ϵ_i is a static offset from the mean used to represent different average properties of individual chromophore molecules, i.e., static inhomogeneity. The width of the distribution of ϵ_i values corresponds to the inhomogeneous width Δ_{in} of the system and quantifies the degree of static disorder in the system. The relative magnitudes and time scales of the underlying dynamics are then described by a normalized time correlation function, $M(t)$, of the time-varying component to the energy transition

$$M(t) = \frac{\langle\delta\omega(0)\delta\omega(t)\rangle}{\langle\delta\omega^2\rangle} \tag{2}$$

where the angled brackets represent an average over the ensemble. When frequencies describing the transition fluctuations are small compared to kT, the $M(t)$ function alone describes the system dynamics. When high-frequency motions, in particular intramolecular vibrations, contribute to the fluctuations, a more complex representation of the $M(t)$ function is needed.[50]

Within the MBO model, all the information required to calculate both the linear signals (e.g., absorption and fluorescence) and the third-order nonlinear signals (e.g., 3PEPS, TG, and TA) are contained in the M(t) correlation function and two corresponding amplitude values: $\langle\delta\omega^2\rangle$ and λ, where λ is the total reorganization energy including both intramolecular vibrational and protein contributions and $\langle\delta\omega^2\rangle$ is the total coupling strength of the system. Once these parameters are determined, a line broadening function, $g(t)$, can be constructed via

$$g(t) = -i\lambda\int_0^t dt_1[1 - M(t_1)] + \langle\delta\omega^2\rangle\int_0^t dt_1\int_0^{t_1} dt_2 M(t_2) \tag{3}$$

The line broadening function can be separated (presuming the molecular motions responsible for the vibrational and the protein dynamics are independent) into vibrational and protein contributions

$$g(t) = g_{protein}(t) + g_{vib}(t) \tag{4}$$

In the case of solvation dynamics studies, the $M(t)$ function is often modeled with a sub-100fs Gaussian decay with several slower exponential decay components;[3,5] however, as we will present in the following sections, we can describe our experimental data with a single Gaussian decay component and no slower decay components

$$M(t) = \lambda_g \exp\left[-\left(\frac{t}{\tau_g}\right)^2\right] \tag{5}$$

In the case of solvation studies, a rapidly decaying Gaussian component is often introduced to describe the inertial motions of the surrounding solvent molecules; in a similar manner we model the rapid relaxation observed in our data as a Gaussian function with a corresponding time constant and amplitude, τ_g and λ_g. For the intramolecular vibrational contribution to the signals, $g_{vib}(t)$ is calculated with the following equation

$$g_{vib}(t) = \sum_i S_i[(\langle n_i\rangle + 1)(\exp(-i\omega_i t - \gamma_i t) - 1) + \langle n_i\rangle(\exp(i\omega_i t - \gamma_i t) - 1) - i\omega_i t] \tag{6}$$

where, $S_i = \Delta_i 2/2$ is the Huang−Rhys factor, Δ_i denotes the dimensionless displacement of the i^{th} mode upon electronic excitation and γ_i is the phenomenological damping constant of the specific vibration. The definition of $M(t)$ from in eq 2 and $g(t)$ from 3 are high-temperature limits. High-frequency vibrational modes do not fall within this approximation and hence we use this more complex representation to describe vibrational contributions to the signals. The thermal occupation number, $<n_i>$, accounts for the thermal population of the modes and is given by

$$\langle n_i\rangle = \frac{1}{\exp\left(\frac{\hbar\omega_i}{k_B T}\right) - 1} \tag{7}$$

Following the construction of the $g(t)$, an induced third-order polarization can be calculated from a convolution of a delta-function response functions, R_i, over the applied laser pulse durations, E_1, E_2, and E_3

$$P^{(3)}(t,T,\tau) = \int_0^\infty dt_3\int_0^\infty dt_2\int_0^\infty dt_1\sum_{i=1}^{4} R_i(t_1,t_2,t_3)E_3(T,t_3)E_2(\tau,t_2)E_1(t_1) \tag{8}$$

Detailed descriptions of the construction of the response functions from the $g(t)$ functions are found in reference.[35] The integrated echo signals measured in the laboratory are subsequently expressed in terms of $P^{(3)}$ via

$$S(T,\tau) = \int_0^\infty dt|\mathrm{P}^{(3)}(t,T,\tau)|^2 \tag{9}$$

In a peak shift experiment, we measure the maximum of the photon echo intensity for a fixed delay T as a function of τ.[5,6]

The peak shift, $\tau^*(T)$, at a particular delay T is defined as the shift of the maximum from $\tau = 0$ of the integrated echo signal. As shown previously,[7] the measured peak shift profiles are directly related to the transition frequency correlation function, $M(t)$, and hence gives direct information on the amplitude and time scales of the fluctuations of the environment and inhomogeneity of the system.

In TA measurements, the first and second interactions originate from the same pulse (pump pulse) and the generated signal is measured in the same direction of the third, detection (probe) pulse. These TA signals are also calculated from $P^{(3)}$ via the following relations

$$I_{TA}(1T) = 2\mathrm{Im}\omega_{pr}\int_{-\infty}^{\infty} dt E_{pr}(t)P^{(3)}(t,T,0) \quad (10)$$

$$= 2\omega_{pr}\int_{-\infty}^{\infty} dt\{\mathrm{Im}(E_{pr}(t)P_{ee}(t,T,0)) + \mathrm{Im}(E_{pr}(t)P_{gg}(t,T,0))\} \quad (11)$$

where ω_{pr} and E_{pr} are the carrier frequency and the field envelope of the probe pulse, respectively. The signal intensity in the TA experiment is directly proportional to the induced optical polarization and is a sum of the ground-state bleach, P_{gg}, and stimulated emission, P_{ee}, contributions. In the experimental data presented here, the detection wavelengths are spectrally separated from the ground-state bleach, and hence the measured signals are free of ground-state bleach contributions.

In the TG experiment, the first and second pulses overlap completely in time ($\tau = 0$) and the TG signal is collected by scanning the T delay. The resulting one-dimensional TG signal is calculated from eq 9 with τ set to 0. In analogy with the TA signals, the TG signals can be separated into contributions from the ground-state polarization, P_{gg}, and the excited states polarization, P_{ee}, but also contain an interference term between these two dynamical polarizations

$$I_{TG}(T) = \int_{-\infty}^{\infty} dt[|P_{ee}(t,T,0)|^2 + |P_{gg}(t,T,0)|^2 + 2\mathrm{Re}\{P_{ee}(t,T,0)P^*_{gg}(t,T,0)\}] \quad (12)$$

The direct interpretation of the TG signals in terms of the constituent ground state and excited state dynamics, without including the interference term has been previously shown to lead to lead to counterintuitive conclusions.[31]

In addition to the time-resolved signals discussed above, the MBO model can be used to calculate the steady-state lineshapes of the system. The absorption lineshape can be calculated from $g(t)$ via

$$\sigma_A(\omega) \propto \mathrm{Re}\int_0^{\infty} dt \exp[i(\omega - \omega_{eg})t - g(t)] \quad (13)$$

and similarly, the fluorescence lineshape is expressed by

$$\sigma_F(\omega) \propto \mathrm{Re}\int_0^{\infty} dt \exp[i(\omega - \omega_{eg} + 2\lambda)t - g^*(t)] \quad (14)$$

Equations 13 and 14 predict lineshapes that are mirror images of each other and shifted by λ from the 0−0 transition and the Stokes shift is given by 2λ. The measured absorption and fluorescence spectra were divided by ω and ω^3 respectively to extract the corresponding lineshapes presented in our study.

We included 29 vibrational modes for the vibrational contributions to our simulations, of which the frequencies and displacements were determined using resonant Raman spectroscopy by Mathies and co-workers.[37] The reorganization energy λ_j associated with the j^{th} mode was calculated from the expression for displaced harmonic oscillators

$$\lambda_j = 1/2\ \omega_j\ \Delta_j^2 \quad (15)$$

and results in a total intramolecular reorganization energy, λ_{vib}, of 1100 cm^{-1}. The TA signals presented here were collected on the red edge of the stimulated emission band and hence excited state vibrations contribute to the signals. In contrast, the 3PEPS signals contain contributions from both ground and excited state vibrations and hence detailed information concerning the vibrational structure in both electronic state is desired. Resonance Raman spectroscopy measures only the frequencies of the intramolecular modes in the ground state, and their corresponding displacements upon excitation, forcing us to use ground-state vibrational parameters in our simulations of both TA and 3PEPS signals. In the case of linear coupling, where no frequency changes in the vibrations occurs upon electronic excitation of the chromophore, this is an applicable premise. However, as we have discussed in the Results section, time-resolved studies suggest the presence of vibrations that do no correlate with the known ground-state vibrational manifold.[25,51] Despite this, to maintain agreement with the Resonance Raman data, we chose to use the frequencies and displacements directly from ref 54.

References and Notes

(1) Lanyi, J. *J. Phys. Chem. B* **2000**, *104*, 11 441−11 448.
(2) Haupts, U.; Tittor, J.; Oesterhelt, D. *Annu. Rev. Biophys. Biomol. Struct.* **1999**, *28*, 367−399.
(3) Fleming, G. R.; Cho, M. H. *Annu. Rev. Phys. Chem.* **1996**, *47*, 109−134.
(4) Stratt, R. M.; Maroncelli, M. *J. Phys. Chem.* **1996**, *100*, 12 981−12 996.
(5) Joo, T. H.; Jia, Y. W.; Yu, J. Y.; Lang, M. J.; Fleming, G. R. *J. Chem. Phys.* **1996**, *104*, 6089−6108.
(6) De Boeij, W. P.; Pshenichnikov, M. S.; Wiersma, D. A. *J. Phys. Chem.* **1996**, *100*, 11 806.
(7) Cho, M. H.; Yu, J. Y.; Joo, T. H.; Nagasawa , Y.; Passino, S. A.; Fleming, G. R. *J. Phys. Chem.* **1996**, *100*, 11 944−11 953.
(8) Jimenez, R.; Fleming, G. R.; Kumar, P. V.; Maroncelli, M. *Nature* **1994**, *369*, 471−473.
(9) Hynes, J. T. In. *Ultrafast Dynamics of Chemical Systems*; Simon, J. D., Ed.; Kluwer Academic Publishers: Dordrecht, 1994, pp 345−381.
(10) Dobler, J.; Zinth, W.; Kaiser, W.; Oesterhelt, D. *Chem. Phys. Lett.* **1988**, *144*, 215−220.
(11) Mathies, R. A.; Brito Cruz, C. H.; Pollard, W. T.; Shank, C. V. *Science* **1988** *240*, 777−779.
(12) Mathies, R. A.; Lin, S. W.; Ames, J. B.; Pollard, W. T. *Annu. Rev. Biophys. Biophys. Chem.* **1991**, *20*, 491−518.
(13) Du, M.; Fleming, G. R. *Biophys. Chem.* **1993** *48*, 101−111.
(14) Atkinson, G. H.; Ujj, L.; Zhou, Y. *J. Phys. Chem. A* **2000**, *104*, 4130−4139.
(15) Rohr, M.; Gartner, W.; Schweitzer, G.; Holzwarth, A. R.; Braslavsky, S. E. *J. Phys. Chem.* **1992**, *96*, 6055−6061.
(16) Doig, S. J.; Reid, P. J.; Mathies, R. A. *J. Phys. Chem.* **1991**, *95*, 6372−6379.
(17) Jäger, F.; Ujj, L.; Atkinson, G. H.; Sheves, M.; Livnah, N.; Ottolenghi *J. Phys. Chem.* **1996**, *100*, 12 066−12 075.
(18) Koyama, Y.; Kubo, K.; Komori, M.; Yasuda, H.; Mukai, Y. *Photochem. Photobiol.* **1991**, *54*, 433−443.
(19) Song, L.; El-Sayed, M. A.; Lanyi, J. K. *Science* **1993**, *261*, 891−894.
(20) Song, L, El-Sayed, M. A. *J. Am. Chem. Soc.* **1998**, *120*, 8889−8890.
(21) Garavelli, M.; Celani, P.; Bernardi, F.; Robb, M. A.; Olivucci, M. *J. Am. Chem. Soc.* **1997**, *119*, 6891−6901.
(22) Hasson, K. C.; Gai, F.; Anfinrud, P. A. *Proc. Natl. Acad. Sci. (USA)* **1996**, *93*, 15 124−15 129.
(23) Haran, G.; Wynne, K.; Xie, A.; He, Q.; Chance, M.; Hochstrasser, R. M. *Chem. Phys. Lett.* **1996**, *261*, 389−395.
(24) Ye, T.; Gershgoren, E.; Friedman, N.; Ottolenghi, M.; Sheves, M.; Ruhman, S. *Chem. Phys. Lett.* **1999**, *314*, 429−434.
(25) Kobayashi, T.; Saito, T.; Ohtani, H. *Nature* **2001**, *414*, 531−534.

(26) Oesterhelt, D.; Stoeckenius, W. *Methods Enzymol.* **1974** *31*, 667−678.
(27) Rouhani, S.; Cartailler J. P.; Facciotti, M. T.; Walian, P.; Needleman, R.; Lanyi, J. K.; Glaeser, R. M.; Luecke, H. *J. Mol. Biol.* **2001**, *313*, 615−628.
(28) Govindjee, R.; Becher, B.; Ebrey, T. *Biophys. J.* **1978**, *22*, 67−77.
(29) Wexler, D.; Kochendoerfer, G. G.; Mathies, R. A. In. *Femtochemistry and Femtobiology: Ultrafast Reaction Dynamics at Atomic Scale Resolution*; Sundstrom, V., Ed.; Imperial College Press: London, 1997, pp 725−752.
(30) Larsen, D. S.; *Rev. Sci. Instr.* **2002**, *73*, 1325−1328.
(31) Larsen, D. S.; Ohta, K.; Yang, M.; Fleming, G. R. *J. Chem. Phys.* **2001**, *114*, 8008−8019.
(32) Joo, T.; Jia, Y.; Yu, J.-Y.; Jonas, D. M.; Fleming, G. R. *J. Phys. Chem.* **1996**, *100*, 2399.
(33) Baltuska, A.; Emde, F. M.; Pshenichnikov, M. S.; Wiersma, D. A. *J. Phys. Chem. A* **1999,** *103,* 10 065−10 082.
(34) Joo, T.; Jia, Y.; Fleming, G. R. *Opt. Lett.* **1995**, *20*, 389.
(35) Haacke, S.; Vinzani, S.; Schenkl, S.; Chergui, M. *ChemPhysChem* **2001**, *2*, 310−315.
(36) Van Grondelle, R.; Dekker: J. P.; Gillbro, T.; Sundstrom, V. *Biochim. Biophys. Acta* **1994**, *1187*, 1−65.
(37) Kroon, A. R.; Hoff, W. D.; Fennema, H. P. M.; Gijzen, J.; Koomen, G. J.; Verhoeven, J. W.; Crielaard, W.; Hellingwerf, K. J. *J. Biol. Chem.* **1996** *271*, 31 949−31 956.
(38) Sasaki, J.; Brown, L. S.; Chon, Y. S.; Kandori, H.; Maeda, A.; Needleman, R.; Lanyi, J. K. *Science* **1995**, *269*, 73−75.
(39) Kolbe, M.; Besir, H.; Essen, L.-O.; Oesterhelt, D. *Science* **2000**, *288*, 1390−1396.
(40) Tittor, J.; Haupts, U.; Haupts, C.; Oesterhelt, D.; Becker, A.; Bamberg, E. *J. Mol. Biol.* **1997**, *271*, 405−416.
(41) Nagasawa, Y.; Yu, J. Y.; Fleming, G. R. *J. Chem. Phys.* **1998**, *109*, 6175−6183.
(42) Yu, J.-Y.; Nagasawa, Y.; van Grondelle, R.; Fleming G. R. *Chem. Phys. Lett.* **1997**, *280*, 404.
(43) Jimenez, R.; van Mourik, F.; Yu, J.-Y.; Fleming, G. R. *J. Phys. Chem. B* **1997** *101*, 7350
(44) Homoelle, B. J.; Edington, M. D.; Diffey, W. M.; Beck, W. F. *J. Phys. Chem. B* **1998**, *102*, 3044−3052.
(45) Agarwal, R.; Krueger, B. P.; Scholes, G. D.; Yang, M.; Yom, J.; Mets, L.; Fleming, G. R. *J. Phys. Chem. B* **2000**, *104*, 2908.
(46) Agarwal, R.; Yang, M.; Xu, Q.-H.; Fleming, G. R. *J. Phys. Chem. B* **2001**, *105*, 1887−1894.
(47) Salverda, J. M.; van Mourik, F.; van der Zwan, G.; van Grondelle, R. *J. Phys. Chem. B* **2000**, *104*, 11 395−11 408.
(48) Groot, M.-L.; Yu, J.-Y.; Agarwal, R.; Norris, J. R.; Fleming, G. R. *J. Phys. Chem. B* **1998**, *102*, 5923−5931
(49) Jordanides, X. J.; Lang, M. L.; Song, X. Y.; Fleming, G. R. *J. Phys. Chem. B* **1999** *103*, 7995.
(50) Ohta, K.; Larsen, D. S.; Yang, M.; Fleming, G. R. *J. Chem. Phys.* **2001**, *114*, 8020−8039
(51) Zinth, W.; Sieg, A.; Huppmann, P.; Blankenhorn, T.; Oesterhelt, D.; Nonella, M. In. *Ultrafast Phenomena XII*, Springer Series in Chem. Physics 66; Elsaesser, T., Mukamel, S., Murnane, M. M., Scherer, N. F., Eds.; Springer Publishing: New York, 2000, 680−682.
(52) Hamm, P.; Zurek, M.; Röschinger, T.; Patzelt, H.; Oesterhelt, D.; Zinth, W. *Chem. Phys. Lett.* **1996**, *263*, 613−621.
(53) Logunov, S. L.; Song, L.; El-Sayed, M. A. *J. Phys. Chem.* **1996**, *100*, 18 586−18 591.
(54) Loppnow, G. R.; Mathies, R. A.; Middendorf, T. R.; Gottfried, D. S.; Boxer, S. G. *J. Phys. Chem.* **1992**, *96*, 737−745.
(55) Xu, Q. H.; Scholes, G. D.; Yang, M.; Fleming, G. R. *J. Phys. Chem. A* **1999**, *103*, 10 348−10 358.
(56) Bradforth, S. E.; Jimenez, R.; Van Mourik, F.; van Grondelle, R.; Fleming, G. R. *J. Phys. Chem.* **1995**, *99*, 16 179.
(57) Vos, M. H.; Jones, M. R.; Hunter, C. N.; Breton, J.; Martin, J. L. *Proc. Natl. Acad. Sci. (USA)* **1994** 12 701−12 705.
(58) Kamalov, V. F.; Masciangioli, T. M.; El-Sayed, M. A. *J. Phys. Chem.* **1996**, *100*, 2762−2765.
(59) Logunov, S. L.; El-Sayed, M. A.; Lanyi, J. K. *Biophys. J.* **1996** *71*, 1545−1553.
(60) Kobayashi, T.; Kim, M.; Taiji, M.; Iwasa, T.; Nakagawa, M.; Tsuda, M. *J. Phys. Chem. B* **1998**, *102*, 272−280.
(61) Arlt, T.; Schmidt, S.; Zinth, W.; Haupts, U.; Oesterhelt, D. *Chem. Phys. Lett.* **1995**, *241*, 559−565.
(62) Changenet-Barret, P.; Choma, C. T.; Gooding, E.F DeGrado, W. F.; Hochstrasser, R. M. *J. Phys. Chem. B* **2000**, *104*, 9322−9329.
(63) Xu, D.; Martin, C. H.; Schulten, K. *Biophys. J.* **1996**, *70*, 453−460.
(64) Mathies, R. A.; Stryer, L. *Proc. Natl. Acad. Sci. (USA)* **1976**, *73*, 2169−2173.
(65) Birge, R. R.; Zhang, C. *J. Chem. Phys.* **1990**, *92*, 7178−7195.
(66) Xu, D.; Schulten, K. *Chem. Phys.* **1994**, *182*, 91−117.
(67) Treutlein, H.; Schulten, K.; Brunger, A. T.; Karplus, M.; Deisenhofer, J.; Michel, H. *Proc. Natl. Acad. Sci. (USA)* **1992**, *89*, 75−79.
(68) Humphrey, W.; Lu, H.; Logunov, I.; Werner, H. J.; Schulten, K. *Biophys. J.* **1998**, *75,* 1689−1699.
(69) Perman, B.; Srajer, V.; Ren, Z.; Teng, T. Y.; Pradervand, C.; Ursby, T.; Bourgeois, D.; Schotte, F.; Wulff, M.; Kort, R.; Hellingwerf, K.; Moffat, K. *Science* **1998**, *279*, 1946−1950.
(70) Subramian, S.; Gerstein, M.; Oesterhelt, D.; Henderson, R. *EMBO J.* **1993**, *12*, 1−8.
(71) Edman, K.; Nollert, P.; Royant, A.; Belrhali, H.; Pebay-Peyroula, E.; Hajdu, J.; Neutze, R.; Landau, E. M. *Nature* **1999**, *401*, 822−826.
(72) Van Aalten, D. M. F.; Hoff, W. D.; Findlay, J. B. C.; Crielaard, W.; Hellingwerf, K. J. *Protein Eng.* **1998**, *11*, 873−879.
(73) Mukamel, S. In. *Principles of Nonlinear Optical Spectroscopy*; Oxford University Press: New York, 1995.